J|A|C|S
ARTICLES

Published on Web 12/15/2008

Cryptophane Xenon-129 Nuclear Magnetic Resonance Biosensors Targeting Human Carbonic Anhydrase

Jennifer M. Chambers,[†] P. Aru Hill,[†] Julie A. Aaron,[†] Zhaohui Han,[‡] David W. Christianson,[†] Nicholas N. Kuzma,[‡] and Ivan J. Dmochowski*[,‡]

Department of Chemistry, University of Pennsylvania, Philadelphia, Pennsylvania 19104, and Department of Biomedical Engineering, University of Rochester, Rochester, New York 14627

Received August 3, 2008; E-mail: ivandmo@sas.upenn.edu

Abstract: ^{129}Xe NMR biosensors are promising agents for early disease detection, especially when their interactions with target biomolecules can perturb ^{129}Xe chemical shifts well beyond the typical field inhomogeneity of clinical MRI. We introduce human carbonic anhydrase (CA) as a single-binding-site enzyme for studying xenon biosensor−protein interactions. A xenon-binding cryptophane was substituted with linkers of varying lengths to *p*-benzenesulfonamide to yield nondiastereomeric biosensors with a single ^{129}Xe NMR resonance. X-ray crystallography confirmed binding of the eight-bond-linked biosensor containing a single xenon atom in the CAII active site. Biosensor dissociation constants (K_d = 20−110 nM) were determined by isothermal titration calorimetry (ITC) for isozymes CA I and II. The biosensor−CA complexes yielded "bound" hyperpolarized ^{129}Xe NMR resonances of narrow line width that were shifted by 3.0−7.5 ppm downfield, signifying much larger shifts than seen previously. Moreover, isozyme-specific chemical shifts clearly differentiated CA I and II, despite their similar structures. Thus, xenon biosensors may provide a powerful strategy for diagnosing human diseases characterized by the upregulation of specific CA isozymes and other protein biomarkers.

Introduction

Magnetic resonance imaging (MRI) is used widely (∼40 million procedures annually) to scan deep tissues in human patients with high spatial resolution. Intrinsic ^{1}H MRI signals from water and fat provide low sensitivity, thus contrast is typically enhanced using gadolinium- or iron-oxide-based agents.[1,2] However, there have been challenges in developing these contrast agents for in vivo imaging of medically relevant biomarkers, such as proteins. Moreover, U.S. and European agencies have recently issued advisories based on studies showing that gadolinium agents pose risks to patients with impaired renal function for developing nephrogenic systemic fibrosis/nephrogenic fibrosing dermopathy (NSF/NFD).[3] These findings motivate the investigation of nonproton-based, hyperpolarized MRI agents such as ^{129}Xe, ^{13}C, and ^{3}He, which enable physiological assays, for example of blood flow and lung function, and provide sensitive methods for studying proteins and metabolites.[4−6]

Functional xenon biosensors have attracted recent attention due to their potential for simultaneously detecting multiple frequency-resolved ^{129}Xe resonances associated with medically relevant biomarkers.[7,8] Monatomic ^{129}Xe is spin-1/2 and exhibits a large chemical shift window (∼300 ppm),[9] while laser polarization enhances ^{129}Xe NMR signals more than 10 000-fold,[10] which helps to compensate for a weaker magnetic moment and much lower concentration of hyperpolarized ^{129}Xe compared to ^{1}H in aqueous solutions. Since the first report of hyperpolarized ^{129}Xe MRI in excised mouse organs,[11] numerous advances in biological imaging with this agent have been made.[12] In a recent study, the xenon gas exchange kinetics of frequency-resolved tissue barrier and red blood cell resonances were measured and used to detect regions of rat lung injury.[13] Frequency-resolved MRI of an immobilized xenon biosensor has also been demonstrated,[14] showing the promise of imaging biosensors bound to a target macromolecule. Most recently, we showed that peptide-functionalized cryptophanes can be deliv-

[†] University of Pennsylvania.
[‡] University of Rochester.

(1) Degani, H.; Gusis, V.; Weinstein, D.; Feilds, S.; Strano, S. *Nat. Med.* **1997**, *3*, 780–782.
(2) Foster-Gareau, P.; Heyn, C.; Alejski, A.; Rutt, B. K. *Mag. Res. Med.* **2003**, *49*, 968–971.
(3) Broome, D. R.; Girguis, M. S.; Baron, P. W.; Cottrell, A. C.; Kjellin, I.; Kirk, G. A. *Am. J. Roentgenol.* **2007**, *188*, 586–592.
(4) Mugler, J. P.; et al. *Magn. Reson. Med.* **1997**, *37*, 809–815.
(5) Golman, K.; Zandt, R. I.; Lerche, M.; Pehrson, R.; Ardenkjaer-Larsen, J. H. *Cancer Res.* **2006**, *66*, 10855–10860.
(6) Hopkins, S. R.; Levin, D. L.; Emami, K.; Kadlecek, S.; Yu, J.; Ishii, M.; Rizi, R. R. *J. Appl. Physiol.* **2007**, *102*, 1244–1254.
(7) Spence, M. M.; Rubin, S. M.; Dimitrov, I. E.; Ruiz, E. J.; Wemmer, D. E.; Pines, A.; Yao, S. Q.; Tian, F.; Schultz, P. G. *Proc. Natl. Acad. Sci. U.S.A.* **2001**, *98*, 10654–10657.
(8) Spence, M. M.; Ruiz, E. J.; Rubin, S. M.; Lowery, T. J.; Winssinger, N.; Schultz, P. G.; Wemmer, D. E.; Pines, A. *J. Am. Chem. Soc.* **2004**, *126*, 15287–15294.
(9) Raftery, D. *Annu. Rep. NMR Spectrosc.* **2006**, *57*, 205–270.
(10) Ruset, I. C.; Ketel, S.; Hersman, F. W. *Phys. Rev. Lett.* **2006**, *96*, 053002.
(11) Albert, M. S.; Cates, G. D.; Driehuys, B.; Happer, W.; Saam, B.; Springer, C. S.; Wishnia, A. *Nature* **1994**, *370*, 199–201.
(12) Cherubini, A.; Bifone, A. *Prog. Nucl. Magn. Res. Spec.* **2003**, *42*, 1–30.
(13) Driehuys, B.; Cofer, G. P.; Pollaro, J.; Mackel, J. B.; Hedlund, L. W.; Johnson, G. A. *Proc. Natl. Acad. Sci. U.S.A.* **2006**, *103*, 18278–18283.
(14) Hilty, C.; Lowery, T. J.; Wemmer, D. E.; Pines, A. *Angew. Chem., Int. Ed.* **2006**, *45*, 70–73.

ered to human cells and achieve intracellular concentrations ($\geq 100\ \mu$M) that should allow in vivo hyperpolarized ^{129}Xe MRI studies.[15]

Herein, we systematically varied the interaction of a xenon biosensor with a biomedically relevant protein, human carbonic anhydrase (CA), in order to investigate whether small changes in binding are detectable by ^{129}Xe NMR. Cryptophane-A-based xenon biosensors offer the possibility of tuning the frequency of the bound ^{129}Xe nucleus, through electronic and mechanical perturbations of the cage environment. Water-soluble cryptophane-A derivatives have been shown to bind xenon with micromolar dissociation constants under nearly physiological conditions, such as in blood plasma.[16] Functionalizing the cryptophane with a biological recognition motif creates a biosensor for the detection of specific proteins, such as matrix metalloproteinases known to be secreted by various tumor cells.[17] Current strategies for constructing protein-targeted xenon biosensors are (i) the use of a peptide to solubilize the large (~1 kD) nonpolar cryptophane[7,8,18] or (ii) the incorporation of cryptophanes into supramolecular dendrimers.[19] While the use of polyamidoamine (PAMAM) dendrimers affords narrow ^{129}Xe line widths, it also shields the cryptophane from solution and renders the bound ^{129}Xe relatively insensitive to protein binding. In contrast, studies with peptido-biotin cryptophane biosensors have shown that decreasing the linker length to the biotin ligand increases the change in chemical shift but also broadens the line width upon avidin binding.[18] Attaching a peptide to the chiral cryptophane creates diastereomers, which increases the number of peaks in the ^{129}Xe spectrum, and correspondingly decreases the signal-to-noise ratio. Computational studies have helped to assign the various NMR resonances to their respective diastereomers.[20] However, the tetrameric nature of avidin can further complicate the ^{129}Xe NMR spectrum.[18]

In the current study, carbonic anhydrase was chosen as the target enzyme due to its biomedical relevance and status as a model system for understanding protein−ligand interactions.[21] CA is involved in many physiological processes such as carbon dioxide transport and pH homeostasis in tissue.[22] However, some CAs also appear to have detrimental effects on human health: For example, CA I, II, and other isozymes were shown to be present and probably involved in the formation of certain tumors and polycystic kidney disease.[23,24] Thus, the development of isozyme-specific CA biosensors holds considerable promise for cancer imaging.

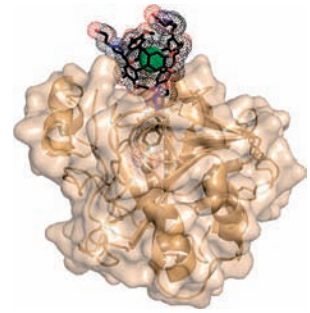

Figure 1. Crystal structure showing **C8B**−Xe−CAII interactions.[29] The Xe atom (green) is shown with a van der Waals diameter of 4.3 Å, the Zn^{2+} ion is gray, the CAII backbone and surface are tan, and the M_oM_o enantiomer of **C8B** is shown in black (carbon), red (oxygen), and blue (nitrogen), surrounded by its van der Waals surface (dots). **C8B** binds in the active site with the sulfonamidate anion coordinated to Zn^{2+}.

Numerous crystal structures of CA−inhibitor complexes are available to guide biosensor development, and CAII in particular has served as a successful model system for rational drug design.[21,25,26] CA is a monomeric protein, which reduces the probability of biosensor−biosensor interactions that were problematic with the tetrameric avidin target.[18] Water-soluble biosensors for CA were developed that avoid the appendage of additional stereocenters to the cryptophane core. Use of the arylsulfonamide ligand allows comparison of the biosensor−CA interaction with other designed CA inhibitors. Solution-based assays for CA can confirm active-site binding, and identify protein−biosensor complexes suitable for crystallization.[27,28] We recently reported the crystal structure of CAII bound to a benzenesulfonamide-linked-cryptophane (Figure 1).[29]

Experimental Procedures

Chemical Synthesis. Synthetic protocols and characterization of all new compounds shown in Scheme 1 can be found in the Supporting Information (Synthetic Methods and Figure S1).

To conjugate the sulfonamide linker to the tripropargyl cryptophane-A cage, 45−90 mg of **1** was dissolved in 2.0−4.0 mL dry DMSO at rt with stirring. Sulfonamide linker **2**, **3**, or **4** (1.1 equiv) was added. A 100 mM $CuSO_4$ solution (0.25 equiv) was added, followed by 2,6-lutidine (0.25 equiv), and 300 mM (+)-sodium-L-ascorbate (0.75 equiv). The reaction was allowed to stir overnight and then poured into 50 mL of H_2O. This solution was extracted with ethyl acetate and the combined organic layer was washed with saturated NaCl solution, dried over Na_2SO_4, filtered, and evaporated. The yellow oil recovered was purified by silica gel column chromatography to give the pure product as a white solid.

Compound **6**, **7**, or **8** (27.2−54.2 mg) was dissolved in 2.0 mL dry DMSO at rt with stirring. **5** (10 equiv) was added. A 100 mM $CuSO_4$ solution (0.25 equiv) was added, followed by 2,6-lutidine (0.25 equiv), and 300 mM (+)-sodium-L-ascorbate (0.75 equiv). The reaction was allowed to stir overnight and then poured into 30 mL of H_2O. Compound **6**, **7**, or **8** was dissolved in dry DMSO at rt with stirring. Solubilizing linker **5** was introduced. A 100 mM $CuSO_4$ solution (0.25 equiv) was added, followed by 2,6-lutidine (0.75 equiv), and 300 mM (+)-sodium-L-ascorbate (0.25 equiv). The reaction was allowed to stir overnight and then poured into

(15) Seward, G. K.; Wei, Q.; Dmochowski, I. J. *Bioconjugate Chem.* **2008**, *19*, 2129–2135.
(16) Hill, P. A.; Wei, Q.; Eckenhoff, R. G.; Dmochowski, I. J. *J. Am. Chem. Soc.* **2007**, *129*, 9262–9263.
(17) Wei, Q.; Seward, G. K.; Hill, P. A.; Patton, B.; Dimitrov, I. E.; Kuzma, N. N.; Dmochowski, I. J. *J. Am. Chem. Soc.* **2006**, *128*, 13274–13283.
(18) Lowery, T. J.; Garcia, S.; Chavez, L.; Ruiz, E. J.; Wu, T.; Brotin, T.; Dutasta, J. P.; King, D. S.; Schultz, P. G.; Pines, A.; Wemmer, D. E. *Chembiochem* **2006**, *7*, 65–73.
(19) Mynar, J. L.; Lowery, T. J.; Wemmer, D. E.; Pines, A.; Frechet, J. M. J. *J. Am. Chem. Soc.* **2006**, *128*, 6334–6335.
(20) Ruiz, E. J.; Sears, D. N.; Pines, A.; Jameson, C. J. *J. Am. Chem. Soc.* **2006**, *128*, 16980–16988.
(21) Krishnamurthy, V. M.; Kaufman, G. K.; Urbach, A. R.; Gitlin, I.; Gudiksen, K. L.; Weibel, D. B.; Whitesides, G. M. *Chem. Rev.* **2008**, *108*, 946–1051.
(22) Supuran, C. T.; Scozzafava, A. *Bioorg. Med. Chem.* **2007**, *15*, 4336–4350.
(23) Pastorekova, S.; Parkkila, S.; Zavada, J. *Adv. Clin. Chem.* **2006**, *42*, 167–216.
(24) Kaneta, S.; Ishizuki, S.; Kasahara, M.; Nagao, S.; Takahashi, H. *Exper. Anim.* **1999**, *48*, 161–169.
(25) Greer, J.; Erickson, J. W.; Baldwin, J. J.; Varney, M. D. *J. Med. Chem.* **1994**, *37*, 1035–1054.
(26) Supuran, C. T. *Nat. Rev. Drug Discovery* **2008**, *7*, 168–181.
(27) Chen, R. F.; Kernohan, J. C. *J. Biol. Chem.* **1967**, *242*, 5813–5823.
(28) Nair, S. K.; Elbaum, D.; Christianson, D. W. *J. Biol. Chem.* **1996**, *271*, 1003–1007.
(29) Aaron, J. A.; Chambers, J. M.; Jude, K. M.; Di Costanzo, L.; Dmochowski, I. J.; Christianson, D. W *J. Am. Chem. Soc.* **2008**, *130*, 6942–6943.

Scheme 1. Synthesis of Trifunctionalized Cryptophane Biosensors **C6B**−**C8B**, M_oM_o Enantiomers Shown[a]

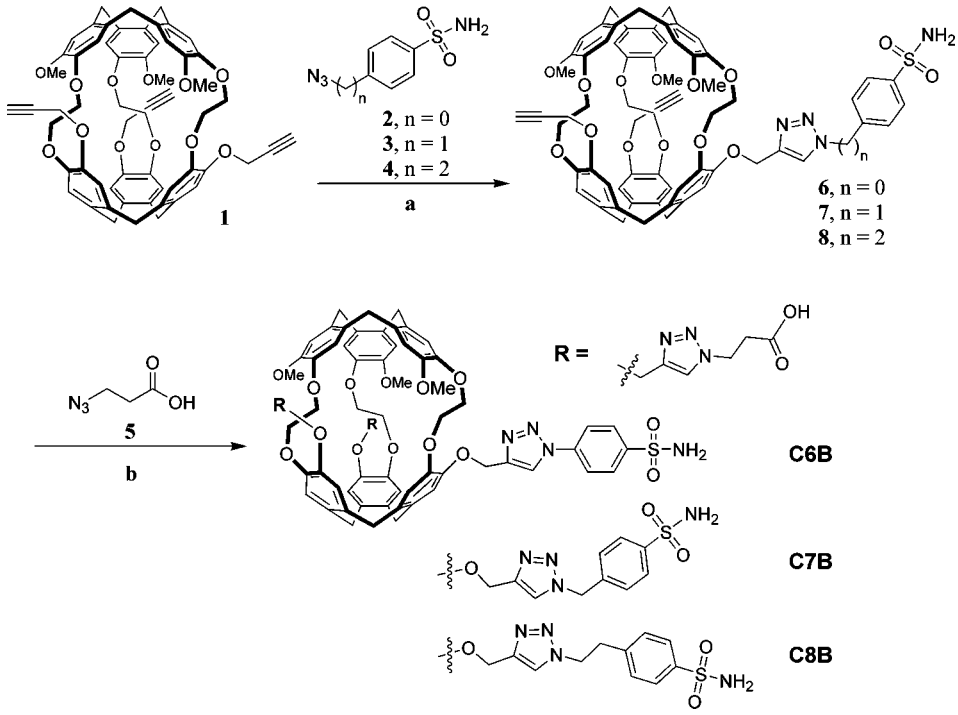

[a] Reagents and conditions for two functionalization steps: (a) Sulfonamide linker (1.1 equiv), 100 mM $CuSO_4$ (0.25 equiv), 2,6-lutidine (0.25 equiv), 300 mM sodium ascorbate (0.75 equiv) 10:1 DMSO/H_2O, 4 h, 41−57% yield; (b) **5** (10 equiv), 100 mM $CuSO_4$ (0.25 equiv), 2,6-lutidine (0.25 equiv), 300 mM sodium ascorbate (0.75 equiv), 10:1 DMSO/H_2O, 12 h, 41−63% yield (17−36% overall yield, as shown, from tripropargyl cryptophane, and 0.8−1.8% overall yield from starting materials).[16]

H_2O. This solution was extracted with ethyl acetate, and the combined organic layer was washed with saturated NaCl solution, dried over Na_2SO_4, filtered, and evaporated. The yellow oil recovered was dissolved in minimal 1 M NaOH, and a white solid was precipitated with the addition of 1 M HCl. The liquid was decanted after a 5-min centrifugation at 13.2 krpm. The solid was then redissolved in minimal 1 M NaOH, precipitated with 1 M HCl, and isolated. The solid was then sonicated for 10 min in DI H_2O and dried under vacuum. If impurities remained, solid was dissolved in minimal CH_2Cl_2 and precipitated with diethyl ether until desired purity was achieved. Pure product was recovered as a white solid.

Isothermal Titration Calorimetry (ITC). All calorimetry experiments were conducted at 298 K on a VP-ITC titration microcalorimeter from MicroCal, Inc. (Northhampton MA), following standard protocols and data analysis.[30,31]

CA I and II were exhaustively dialyzed against 50 mM Tris-SO_4 (pH 8.0). Compounds (∼10 mM stock solution in DMSO) were dissolved at a concentration of 135−300 μM in an aliquot of the same buffer, and an equivalent volume of DMSO was added to the enzyme solution. Prior to the titration experiment, samples were degassed under vacuum for 5 min. The sample cell (effective volume = 1.4 mL) was overfilled with 1.8 mL of CA at a concentration of 14−26 μM, and the reference cell was filled with water. The contents of the sample cell were titrated with 30 aliquots (10 μL each) of inhibitor (two initial 2 μL injections were made, but not used in data analysis). After each injection, the heat change was measured and converted to the corresponding enthalpy value. The reaction mixture was continuously stirred at 300 rpm during titration. Control experiments were carried out by titrating the inhibitor into the buffer solution under identical experimental conditions. The calorimetric data are presented with the background titrations subtracted from the experimental data. The amount of heat produced per injection was calculated by integration of the area under each peak. Data were fit to the equation $q = V\Delta H[E]_t K[L]/(1 + K[L])$, where q is the heat evolved during the course of the reaction, V is the cell volume, ΔH is the binding enthalpy per mole of ligand, $[E]_t$ is the total enzyme concentration, K is the binding constant, and [L] is inhibitor concentration. Nonlinear regression fitting to the binding isotherm (ORIGIN 5.0 software, MicroCal) using a one-site model gave the equilibrium dissociation constant of the ligand, K_d, and estimates of the standard error, as provided in Table 1. The error is $\sigma_i = \sqrt{(C_{ii}\chi^2)}$, where C_{ii} is the diagonal element of the variance-covariance matrix.

Table 1. Dissociation Constants for CA−Linker and CA−Biosensor Complexes at 298 K

enzyme	ligand	K_d (nM)
CAI	**4**	30 ± 10
	C6B	20 ± 10
	C7B	80 ± 10
	C8B	30 ± 20
CAII	**4**	100 ± 10
	C6B	100 ± 20
	C7B	110 ± 30
	C8B	60 ± 20

Hyperpolarized ^{129}Xe NMR Spectroscopy. Isotopically enriched xenon (86% ^{129}Xe and 0.13% ^{131}Xe, Spectra Gases) was polarized via spin-exchange optical pumping with rubidium at 175 °C[32] and cryogenically separated[33] from the buffer-gas mixture (1% Xe, 10% N_2, 89% He by volume) in a Nycomed−Amersham (now GE) IGI.Xe.2000 gas-flow polarizer (output ^{129}Xe polarization 10−20% for 300-mL batches of pure xenon gas). Immediately after

(30) Wiseman, T.; Williston, S.; Brandts, J. F.; Lin, L. N. *Anal. Biochem.* **1989**, *179*, 131–137.
(31) Fisher, H. F.; Singh, N. *Methods Enzymol.* **1995**, *259*, 194–221.
(32) Walter, D. K.; Griffith, W. M.; Happer, W. *Phys. Rev. Lett.* **2001**, *86*, 3264–3267.
(33) Kuzma, N. N.; Patton, B.; Raman, K.; Happer, W. *Phys. Rev. Lett.* **2002**, *88*, 147602.

thawing, xenon was transferred to a special aluminum container inside a home-built ^{129}Xe probe in the bore of a 9.4 T superconducting magnet (Oxford Instruments). Spin relaxation time, T_1, of ^{129}Xe gas in the container ranged from 70 to 120 min.

Hyperpolarized ^{129}Xe NMR measurements[12] with water-soluble cryptophane biosensors were performed similarly to our previous studies,[17] with the exception of frequency-shift referencing described below. For experiments not involving CA, 650 μL solutions of **C6B** (96 μM), **C7B** (186 μM), or **C8B** (121 μM) in 50 mM Tris-SO_4 water-based buffer (pH 8.0) were added to a 5-mm NMR tube fitted vertically onto a removable probe. A 1-mm outer diameter glass capillary was inserted into the NMR tube to allow bubbling of hyperpolarized Xe gas through the sample. NMR samples were interchanged without removing the hyperpolarized Xe container from the vertical magnet bore.

After thermal equilibrium inside the magnet had been achieved (temperature range for all experiments was 20.0−20.5 °C, with thermal fluctuation of only 0.1 °C), hyperpolarized Xe gas was bubbled through the biosensor solution for ∼1 min, and the ^{129}Xe@cryptophane signal was monitored via a 1−5 μs pulse every 10 s. Once the ^{129}Xe@cryptophane signal indicated saturation, Xe bubbling was stopped, and four pulses at 7−11 μs were used to obtain data ($n = 4$, ^{129}Xe frequency $f_0 = 110.74668$ MHz, 40−70° tipping pulse) and then averaged. Raw free induction decay (FID) signals were recorded in quadrature. Where useful, multiple processed spectra were averaged to increase signal-to-noise ratio. The biosensor−CA samples were prepared in 50 mM Tris-SO_4 buffer (pH 8.0) using the following concentrations: **C6B** (188 μM) + CAI (141 μM), **C6B** (148 μM) + CAII (123 μM), **C7B** (136 μM) + CAI (100 μM), **C7B** (132 μM) + CAII (105 μM), **C8B** (189 μM) + CAI (141 μM), and **C8B** (189 μM) + CAII (153 μM). The biosensor−CA samples were then subjected to the same data collection procedure as the unbound biosensor samples. NMR data were processed using standard fast Fourier transform combined with baseline and phase corrections. Spectra were fitted to linear combinations of Lorentzians using IGOR Pro 5.0 (Wavemetrics, Inc., Oregon). Gaussian broadening of 20 Hz was applied to obtain the shown spectra, however the fits were done without any broadening.

A new procedure, detailed in the Supporting Information (^{129}Xe NMR Methods) was used to reference NMR frequencies to the ^{129}Xe gas line. In the low-frequency region, two narrow ^{129}Xe peaks (from the gas in the vertical capillary and in the spherical bubbles) were observed, superimposed on a broad peak from the gas above the liquid surface. As xenon bubbling was stopped, the down-frequency peak from the bubbles disappeared, and all other peaks shifted by −31 Hz (−0.3 ppm). The narrow gas peaks were split diamagnetically by 343 ± 20 Hz (3.1 ± 0.2 ppm), consistent with $-(s_{cyl} - s_{sph})\chi_w = 3.01$ ppm, where $s_{cyl} = 1$ and $s_{sph} = 2/3$ are magnetization shape factors for a vertical cylinder and a sphere, and χ_w is diamagnetic susceptibility of the surrounding solution based on water (−9.04 ppm in SI units). Because the chemical shift of ^{129}Xe gas at 20.2 °C and 1 atm is 0.509 ppm relative to ^{129}Xe gas at 0 atm,[34] we used the following expression to convert peak frequencies f to ppm: σ [ppm] $= 10^6(f - f_c + 343)/f_0 + 0.509$, where f_c is the measured peak frequency of ^{129}Xe gas in the capillary and f_0 is the spectrometer frequency, both in Hz. The uncertainties in ^{129}Xe chemical shifts from peak fits were small (∼4 Hz, 0.04 ppm), with additional sources of error (such as the fit to the gas reference peak) being comparable or smaller. These contributions resulted in peak uncertainties of ∼ ±0.07 ppm. ^{129}Xe chemical shifts are reported to a precision of ±0.1 ppm. The calculated ^{129}Xe NMR chemical shifts for biosensor **C7B** were decreased by 0.1 ppm to compensate for the slightly higher temperatures (20.3−20.46 °C, see Table S1) at which these data were collected, using the measured temperature dependence of −0.28 ppm/°C.[18]

Results

Biosensor Design and Synthesis. Unlike prior biotin-functionalized Xe biosensors, which gained water solubility through the attachment of a chiral peptide,[7,8,18] biosensors for CA were designed to avoid the incorporation of tetrahedral stereocenters. Parent cryptophane-A is chiral, with D_3 symmetry,[35] as the top and bottom cyclotriveratrylene moieties are oriented in an anti configuration. With the original biotin-labeled Xe biosensor, the use of chiral peptide and maleimide-functionalized biotin-generated four diastereomers,[8] which was later reduced to two diastereomers through direct coupling of the biotin to an orthogonally protected lysine residue.[18] In each case, avidin binding typically produced numerous overlapping, and correspondingly broadened resonances. In targeting CA, biosensors were modeled into CAII and structures were identified that allowed coordination of the sulfonamidate anion to the active-site Zn^{2+}. We designed relatively low molecular weight biosensors (1372−1423 g/mol, not including Xe), in order to maximize rotational mobility, and achieve narrow hyperpolarized ^{129}Xe NMR resonances. Scheme 1 shows cryptophanes attached via triazole linkers with 6-, 7-, and 8-bonds to benzenesulfonamide (**C6B**, **C7B**, **C8B**). The shortest biosensor, **C6B** fit inside the protein cleft and positioned the cryptophane edge at the protein surface, ∼15 Å from the Zn^{2+} active site. Longer biosensors **C7B** and **C8B** were conceived as a way to modulate the interaction between the protein and cryptophane and to observe the resulting changes in ^{129}Xe NMR chemical shift. Modeling studies were validated by the X-ray crystal structure determination of **C8B**-CAII (Protein Data Bank accession code 3CYU, Figure 1), which used anomalous scattering information to confirm the encapsulation of Xe within the cryptophane.[29]

Benzenesulfonamide was *para*-substituted with azido-functionalized linkers **2**−**4** that were readily synthesized from the amine analogues (see Supporting Information, Synthetic Methods), and provided a variable 6−8 bond spacer between the cryptophane and benzenesulfonamide recognition unit. As seen in Scheme 1, linkers **2**−**4** were reacted with tripropargyl cryptophane (**1**) by a copper (I)-catalyzed [3 + 2] cycloaddition process previously developed by others[36,37] and applied by our laboratory.[16,17] It was determined that **2** was degraded with light when dissolved in DMSO; thus, conjugate **6** was successfully synthesized in the absence of light. Conjugates **7** and **8** did not require this additional precaution.

Compounds **6**−**8** exhibited poor solubility in aqueous media. To enable subsequent solution NMR and crystallography experiments, two carboxylic acid groups were attached to the cryptophane. 3-Azidopropionic acid **5** was readily prepared following literature protocols[38] and reacted in 5-fold excess with the two remaining alkynes by the same copper (I)-catalyzed [3 + 2] cycloaddition process. In neutral aqueous solutions, the dianionic biosensors **C6B**−**C8B** exhibited favorable solubility for X-ray crystallography studies with CAII.

Biosensor Binding Studies. Initial binding studies were conducted using a dansylamide displacement assay,[27,28] which

(34) Jameson, C. J.; Jameson, A. K.; Cohen, S. M. *J. Chem. Phys.* **1973**, *59*, 4540–4546.
(35) Collet, A. *Comp. Supramol. Chem.* **1996**, *2*, 325–365.
(36) Tornoe, C. W.; Christensen, C.; Meldal, M. *J. Org. Chem.* **2002**, *67*, 3057–3064.
(37) Rostovtsev, V. V.; Green, L. G.; Fokin, V. V.; Sharpless, K. B. *Angew. Chem., Int. Ed.* **2002**, *41*, 2596–2599.
(38) Leffler, J. E.; Temple, R. D. *J. Am. Chem. Soc.* **1967**, *89*, 5235–5246.

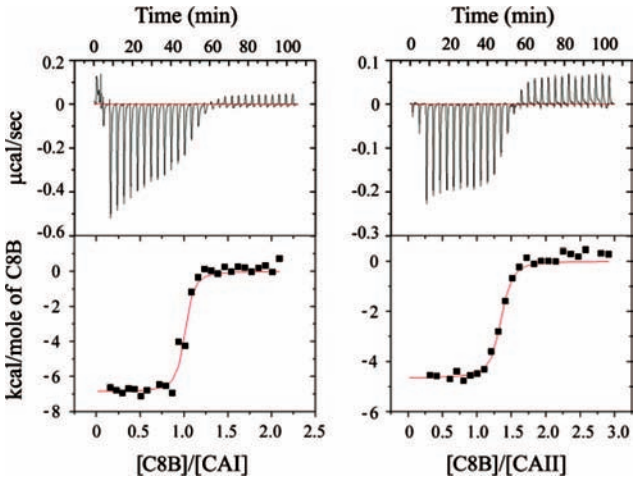

Figure 2. Representative ITC experiment with enthalpograms for CA−biosensor complexation at 298 K in 50 mM Tris buffer, pH 8.0. (left) CAI (14.2 μM) titrated with **C8B** (135.7 μM); (right) CAII (14.9 μM) titrated with **C8B** (200.0 μM).

confirmed biosensor binding to the active sites of CA I and II in solution (data not shown). Isothermal titration calorimetry was used to determine the affinity of binding of **4**, **C6B**, **C7B**, and **C8B** to CA I and II (Figure 2 and Table 1). Biosensor **C8B** exhibited higher affinity for CAII than the other compounds. However, all four compounds bound slightly better to CAI, with **C6B** exhibiting the highest affinity for CAI and 5-fold discrimination over CAII. Further discrimination may be possible by varying the linker joining benzenesulfonamide and cryptophane, based on small differences between the isozymes in active-site architecture.[39,40] Data in Table 1 indicate that the cryptophane and tether length had little effect on the CA I and II dissociation constants (K_d = 20−110 nM) for this range of linkers. Larger refined thermal (B) factors for **C8B** ($\langle B \rangle$ = 42 Å^2) compared with the overall CAII model ($\langle B \rangle_{\text{main chain}}$ = 31 Å^2; $\langle B \rangle_{\text{side chain}}$ = 35 Å^2) reflect the mobility and conformational heterogeneity of the bound biosensor.[29] Indeed, the cryptophane in **C8B** sits a few angstroms above the active-site cleft, and there are few hydrogen bonds or other specific interactions with the protein. These structural data are consistent with the relative insensitivity of affinity to tether length. A more detailed investigation into the thermodynamics of the biosensor−protein interaction will be reported in due course.

Hyperpolarized ^{129}Xe NMR Spectroscopy. As expected, the racemic mixture of unbound M_oM_o and P_oP_o enantiomers produced a single isotropic peak for **C6B** (63.5 ppm), **C7B** (63.9 ppm), and **C8B** (62.9 ppm) in their hyperpolarized ^{129}Xe NMR spectra (Figure 3a, d, g and Table 2).[20] In the presence of substoichiometric CA, the ^{129}Xe NMR peak corresponding to unbound biosensor was typically shifted 0.2−0.4 ppm downfield, which reflects differences in solution properties.

Trials with the three biosensors demonstrated repeatable and significant changes in ^{129}Xe NMR chemical shift upon addition of CA I or II. Addition of CAI to **C8B** gave an unbound resonance at 63.3 ppm and two peaks at 67.9 and 66.3 ppm for the bound enantiomers (Figure 3h), with $\Delta\delta$ = 4.5 and 3.0 ppm. The spectrum of **C8B** with CAII (Figure 3i) gave an unbound resonance at 63.2 ppm and also showed two resonances for the bound cryptophane enantiomers, with the first at 68.2 ppm ($\Delta\delta$ = 5.0 ppm) and the second at 66.9 ppm ($\Delta\delta$ = 3.7 ppm). The difference between the peaks observed for **C8B** when bound to CAI (1.5 ppm) and CAII (1.3 ppm) are at the upper bound of the values observed by Lowery et al. for the diastereomeric biotin-labeled cryptophanes bound to avidin.[18] The paired resonances observed for **C8B** are also likely diastereomeric in nature, based on differences in the chiral potential of ^{129}Xe in the two enantiomers bound to the chiral protein. The protein crystal structure identifies one possible site of interaction between **C8B** and CAII, with the M_oM_o and P_oP_o enantiomers occupying very similar positions around a central xenon atom.[29]

Interestingly, the laser-polarized ^{129}Xe NMR spectrum of **C6B** with CAI (Figure 3b) showed only a single peak for bound cryptophane biosensor at 69.2 ppm with the unbound peak at 63.7 ppm ($\Delta\delta$ = 5.6 ppm). The spectrum of **C6B** with CAII (Figure 3c) also showed a single peak for bound cryptophane, at 68.2 ppm, with the unbound peak at 63.1 ppm ($\Delta\delta$ = 5.1 ppm). On the basis of previous results with biotin-labeled biosensors, it was expected that the short linker of **C6B** would cause a strong binding-induced shift on the encapsulated ^{129}Xe resonance due to the proximity of the biosensor to the protein.[18] It was not expected, however, that **C6B** bound to CA I or II would exhibit only a single bound ^{129}Xe resonance. Diastereomerically resolved resonances were previously identified in Lowery's biotin-linked cryptophanes, and were also observed in **C8B**−CA. It is not possible that only a single enantiomer of **C6B** is binding CA, based on the stoichiometries obtained from ITC measurements (see Supporting Information, Figure S2). These data and the relatively narrow (40 ± 10 Hz) ^{129}Xe@**C6B**−CA line width, indicate that the two enantiomers of **C6B** must induce the same change in the potential of the ^{129}Xe nucleus when bound to the chiral protein pocket. In addition to the single "bound" peak, the short linker of **C6B** provides significantly larger chemical shift changes compared to the previous biosensors that targeted avidin,[18] without sacrificing line width.

The laser-polarized ^{129}Xe NMR spectrum of **C7B** with CAI (Figure 3e) also showed only a single peak for bound cryptophane biosensor at 66.9 ppm with the unbound peak at 63.7 ppm ($\Delta\delta$ = 3.2 ppm). Most interestingly, when complexed with CAII (Figure 3f), **C7B** showed a bound resonance at 67.0 ppm, and a second bound resonance at 71.2 ppm ($\Delta\delta$ = 7.5 ppm, relative to the unbound resonance at 63.7 ppm). This shift is the largest ever reported for a xenon biosensor. Moreover, the peak at 71.2 ppm for **C7B**−CAII clearly provides isozyme discrimination between CA I and II, which creates opportunities for ^{129}Xe NMR multiplexing experiments.

The observation of a single "bound" peak for **C6B**−CAI, **C6B**−CAII, and **C7B**−CAI (Table 2) suggests that this is a common feature of xenon biosensors when the cryptophane is confined by a rigid linker within the CA environment. The cryptophane in close proximity to CA will be partially desolvated and experience a lower dielectric environment[29] but is not expected to bind to the protein surface. The net environmental changes felt by the xenon in this case appear to dominate the observed ^{129}Xe NMR chemical shift and outweigh diastereomeric considerations.

In an attempt to explain the spectral differences between **C7B**−CAI (one "bound" peak) and **C7B**−CAII (two "bound" peaks), we inspected the two isozyme sequences. Using

(39) Turkmen, H.; Durgun, M.; Yilmaztekin, S.; Emul, M.; Innocenti, A.; Vullo, D.; Scozzafava, A.; Supuran, C. T. *Bioorg. Med. Chem. Lett.* **2005**, *15*, 367–372.
(40) Srivastava, D. K.; Jude, K. M.; Banerjee, A. L.; Haldar, M.; Manokaran, S.; Kooren, J.; Mallik, S.; Christianson, D. W. *J. Am. Chem. Soc.* **2007**, *129*, 5528–5537.

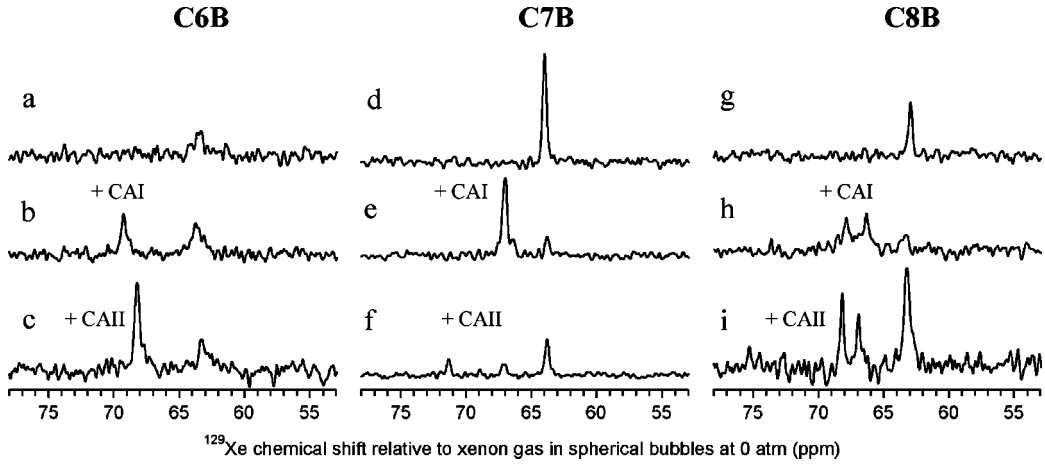

Figure 3. Laser-polarized ^{129}Xe NMR spectra with biosensors in 50 mM Tris, pH 8.0, buffer solution. (a,d,g) ^{129}Xe NMR spectra showing individual biosensors free in solution, (b,e,h) ^{129}Xe NMR spectra showing each biosensor bound to CAI. (c,f,i) ^{129}Xe NMR spectra showing each biosensor bound to CAII. (a) **C6B** alone (96 μM); (b) **C6B** (188 μM) and CAI (141 μM); (c) **C6B** (148 μM) and CAII (123 μM); (d) **C7B** alone (186 μM); (e) **C7B** (136 μM) and CAI (100 μM); (f) **C7B** (132 μM) and CAII (105 μM); (g) **C8B** alone (121 μM); (h) **C8B** (189 μM) and CAI (141 μM); (i) **C8B** (189 μM) and CAII (153 μM).

Table 2. ^{129}Xe NMR Chemical Shifts for **C6B**, **C7B**, and **C8B** Free in Solution, Bound to CA I or II

biosensor	unbound [ppm]	CAI [ppm] unbound; bound	Δ CAI [ppm]	CAII [ppm] unbound; bound	Δ CAII [ppm]
C6B	63.5	63.7; 69.2	5.6	63.1; 68.2	5.1
C7B	63.9	63.7; 66.9	3.2	63.7; 71.2; 67.0	7.5, 3.3
C8B	62.9	63.3; 67.9, 66.3	4.5, 3.0	63.2; 68.2, 66.9	5.0, 3.7

[a] **C7B** data were temperature corrected by subtracting 0.1 ppm in order to match ^{129}Xe NMR data for C6B and **C8B**.

EMBOSS-Align:Needle, CA I and II were found to have high sequence identity (60%) and sequence similarity (72%).[41] Structural homology (rmsd = 0.92 Å) was calculated using the TOP3D program of the CCP4 package,[42] with ligand-free crystal structures for CAI (Protein Data Bank accession code 2CAB),[43] and CAII (Protein Data Bank accession code 2CBA).[44] CA I and II possess active-site clefts of virtually identical width (15 Å) and depth (15 Å).[40] Thus, the 10-Å diameter cryptophane must experience similar steric environments in the two CA isozymes.

Despite these structural similarities, the cavities of CA I and II vary considerably in the distribution of polar and nonpolar residues. For example, two hydrophobic patches that are unique to the CAII active-site channel previously guided the synthesis of high-affinity enzyme inhibitors.[45] These patches, as well as other sites rich in aromatic residues, are accessible to the Zn^{2+}-bound cryptophane biosensor and may serve to discriminate between the enantiomers of **C7B**. We hypothesize that in **C7B**−CAI, the bound enantiomers produce equivalent ^{129}Xe NMR resonances by being in close proximity to the protein environment, whereas in **C7B**−CAII, cryptophane interactions with the protein surface lead to diastereomerism. The variation in ^{129}Xe NMR chemical shift observed for the two enantiomers of **C7B**−CAII ($\Delta\delta$ = 4.2 ppm) compared to **C8B**−CAII ($\Delta\delta$ = 1.3 ppm) may be due to conformational differences between the two biosensors. In **C7B**, the benzenesulfonamide is kinked by 109° relative to the linker, which may enforce interactions of one or both enantiomers with the protein surface.

Importantly for biosensing applications, the line widths of "bound" xenon biosensors (23−50 Hz) were only somewhat broadened compared to free xenon in solution (12 ± 1 Hz) and were relatively unchanged from the "free" xenon biosensors **C7B** (27 ± 1 Hz) and **C8B** (25 ± 3 Hz). The apparently broader line width of **C6B** (79 ± 20 Hz) was likely the result of poor mixing and low cryptophane-bound hyperpolarized ^{129}Xe NMR signal. Nonetheless, all three biosensors exhibited excellent solubility in aqueous solutions. In the crystal structure of **C8B**−CAII,[29] the enantiomers appear to interact very little with the CAII surface, which should allow rotational and translational motions of the biosensor, and promote narrow NMR line widths. Furthermore, because the cryptophane in **C8B**−CAII appears to be unperturbed by the protein,[29] the xenon within the cryptophane can continue to behave isotropically. This should make the noncovalently bound ^{129}Xe nucleus fairly insensitive to the larger rotational correlation time of the biosensor−CA complex. By comparison, the previous use of polypeptide solubilizing moieties and linkers in biotin-functionalized biosensors may have promoted binding interactions with avidin that contributed to line-broadening.[18] The CA data support the design of minimally chiral, low-molecular-weight ^{129}Xe biosensors that target proteins with single binding sites while minimizing binding interactions between the cryptophane−linker and the protein surface.

Discussion

In cancer patients, tumors can exist for long periods in a dormant, asymptomatic state before development and diagnosis of disease.[46] Furthermore, human cancers are characterized by the overexpression of many different proteins.[47] Thus, the ability to detect the overexpression of multiple protein biomarkers that co-localize and identify a population of abnormal cells has the potential to vastly improve the accuracy and efficacy of early cancer detection.

(41) Rice, P.; Longden, I.; Bleasby, A. *Trends Genet.* **2000**, *16*, 276–277.
(42) , *Acta Crystallogr.* **1994**, *D50*, 760–763, CCP4 Collaborative Project.
(43) Kannan, K. K.; Ramanadham, M.; Jones, T. A. *Ann. N.Y. Acad. Sci.* **1984**, *429*, 49–60.
(44) Hakansson, K.; Carlsson, M.; Svensson, L. A.; Liljas, A. *J. Mol. Biol.* **1992**, *227*, 1192–1204.
(45) Jain, A.; Whitesides, G. M.; Alexander, R. S.; Christianson, D. W. *J. Med. Chem.* **1994**, *37*, 2100–2105.
(46) Almog, N.; Henke, V.; Flores, L.; Hlatky, L.; Kung, A. L.; Wright, R. D.; Berger, R.; Hutchinson, L.; Naumov, G. N.; Bender, E.; Akslen, L. A.; Achilles, E.-G.; Folkman, J. *FASEB J.* **2006**, *20*, 947–949.

Toward this goal, we have shown that water-soluble ^{129}Xe NMR biosensors can be targeted with nanomolar affinity to biomedically relevant proteins, human carbonic anhydrases I and II. A xenon-binding tripropargyl cryptophane was functionalized in two facile copper(I)-catalyzed [3 + 2] cycloaddition steps, where the linker to benzenesulfonamide was varied between 6 and 8 bonds. X-ray crystal structure analysis of CAII complexed with **C8B** confirmed ligation of the sulfonamide moiety to Zn^{2+} in the CA active site, with the cryptophane at the upper rim of the active-site cleft. CA is the first monomeric, single-binding-site protein that has been studied with a xenon biosensor. ITC measurements revealed that **C6B**, **C7B**, and **C8B** exhibit similar dissociation constants for CA as the bare linker **4**, indicating that the cryptophane has little effect on CA binding affinity for this range of linkers.

CA serves as a useful model system for studying xenon biosensor−protein interactions. In order to improve detection sensitivity, HyperCEST technique[48,49] was proposed to irradiate and selectively quench the hyperpolarized ^{129}Xe NMR signal(s) corresponding to the bound species. The presence of a biomarker would be detected as a decrease in the bulk ^{129}Xe NMR signal, based on rapid exchange between xenon populations. ^{129}Xe NMR peaks with narrow line widths and large changes in chemical shift will facilitate selective irradiation of one or more "bound" xenon species in solution, as required for indirect detection. Additionally, well-resolved resonances will facilitate direct detection. ^{129}Xe NMR studies with **C6B**, **C7B**, and **C8B** indicated significant and reproducible downfield shifts of 5.6, 7.5, and 5.0 ppm upon binding to CA, which are considerably larger than those observed previously for ^{129}Xe biosensors targeting avidin.[18] The magnitude of the shifts, relative to typical MRI field inhomogeneity of ∼1 ppm,[50] holds considerable promise for in vivo imaging studies.

Finally, isozyme discrimination was observed for all three ^{129}Xe biosensors, with a ^{129}Xe NMR chemical shift difference of ∼0.5 ppm between **C6B**−CAI and **C6B**−CAII and between **C8B**−CAI and **C8B**−CAII. Significantly, a peak was observed exclusively for **C7B**−CAII that was 4.3 ppm downfield from the single bound resonance for **C7B**−CAI. Isozyme-specific chemical shifts clearly differentiate between CA I and II, despite their homologous structures.

Conclusion

In summary, we synthesized ^{129}Xe NMR biosensors for CA I and II by modifying a cryptophane-A cage with two water-solubilizing groups and attaching an arylsulfonamide recognition moiety via a triazole linker. The linker was varied between 6 and 8 bonds, in order to tether the biosensors to active-site Zn^{2+} and modulate the interaction between cryptophane and CA. ITC confirmed nanomolar affinity for CA I and II. When bound to CA, biosensors **C6B**, **C7B**, and **C8B** demonstrated repeatable changes in ^{129}Xe chemical shifts of 5.6, 7.5, and 5.0 ppm, with 7.5 ppm being the largest chemical shift change ever reported for a xenon biosensor. CA I and II were distinguished by **C6B** and **C8B** by reproducible 0.5 ppm chemical shift differences. Remarkably, **C7B** produced a unique resonance when bound to CAII that was shifted 4.3 ppm downfield from the resonance assigned to CAI. On the basis of the design principles that have been advanced through this work, xenon biosensors now provide avenues for detecting diseases associated with CA and other proteins by in vivo hyperpolarized ^{129}Xe NMR spectroscopy.

Acknowledgment. This work was supported by an NIH Chemical Biology Interface training grant to J.A.A., NIH Grant No. GM49758 to D.W.C., and DOD (W81XWH-04-1-0657), NIH (1R21CA110104), and Camille and Henry Dreyfus Teacher-Scholar awards to I.J.D. We thank Ronen Marmorstein and Jeffery Saven for access to instrumentation, and Luigi Di Costanzo, George Furst, and M.G. Finn for valuable discussions. Thanks go to Kevin Jude for providing CAII, and Garry Seward and Jan-Oliver Janda for experimental assistance.

Supporting Information Available: Complete ref 4, detailed synthetic methods and compound characterization, ^{129}Xe NMR methods, ^{129}Xe NMR data set parameters and full spectrum, ITC data for **4**, **C6B**, and **C7B**. This material is available free of charge via the Internet at http://pubs.acs.org.

JA806092W

(47) Welsh, J. B.; Sapinoso, L. M.; Kern, S. G.; Brown, D. A.; Liu, T.; Bauskin, A. R.; Ward, R. L.; Hawkins, N. J.; Quinn, D. I.; Russell, P. J.; Sutherland, R. L.; Breit, S. N.; Moskaluk, C. A.; Henry, F.; Frierson, J.; Hampton, G. M. *Proc. Natl. Acad. Sci. U.S.A.* **2003**, *100*, 3410–3415.
(48) Schroder, L.; Lowery, T. J.; Hilty, C.; Wemmer, D. E.; Pines, A. *Science* **2006**, *314*, 446–449.
(49) Garcia, S.; Chavez, L.; Lowery, T. J.; Han, S.-I.; Wemmer, D. E.; Pines, A. *J. Magn. Reson.* **2007**, *184*, 72–77.
(50) Gillies, R. J.; Morse, D. L. *Annu. Rev. Biomed. Eng.* **2005**, *7*, 287–326.